Inorganic Chemistry

Article

pubs.acs.org/IC

Using Functionalized Silyl Ligands To Suppress Solvent Coordination to Silyl Lanthanide(II) Complexes

Rainer Zitz,[†] Johann Hlina,[†] Mohammad Aghazadeh Meshgi,[†] Heinz Krenn,*[,‡] Christoph Marschner,*[,†] Tibor Szilvási,*[,§] and Judith Baumgartner*[,∥]

[†]Institut für Anorganische Chemie, Technische Universität Graz, Stremayrgasse 9, 8010 Graz, Austria

[‡]Institut für Physik, Fachbereich Experimentalphysik, Magnetometry und Photonics, Universität Graz, Universitätsplatz 5, 8010 Graz, Austria

[§]Department of Chemical & Biological Engineering, University of Wisconsin—Madison, 1415 Engineering Drive, 53706 Madison, Wisconsin, United States

[∥]Institut für Chemie, Universität Graz, Stremayrgasse 9, 8010 Graz, Austria

Supporting Information

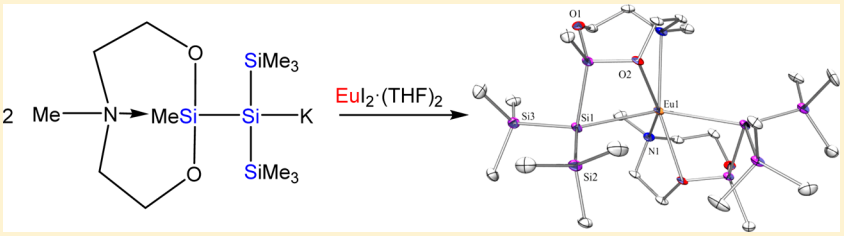

ABSTRACT: The reaction of the potassium 1,3-trisilanediide $Me_2Si[Si(Me_3Si)_2K]_2$ with SmI_2 and YbI_2 was found to give the respective disilylated complexes $Me_2Si[Si(Me_3Si)_2]_2Sm{\cdot}2THF$ and $Me_2Si[Si(Me_3Si)_2]_2Yb{\cdot}2THF$. Desolvation of coordinated solvent molecules in these complexes made their handling difficult. However, using a number of functionalized silanide ligands, complexes with a diminished number or even no coordinated solvent molecules were obtained ($(R_3Si)_2Ln(THF)_x$ (x = 0−3)). The structures of all new lanthanide compounds were determined by X-ray single-crystal structure analysis. NMR spectroscopic analysis of some Yb−silyl complexes pointed at highly ionic interactions between the silyl ligands and the lanthanides. This bonding picture was supported by DFT calculations at the B3PW91/Basis1 level of theory. Detailed theoretical analysis of a disilylated Eu(II) complex suggests that its singly occupied molecular orbitals (SOMOs) are very close in energy to the ligand silicon lone pairs (HOMO), and SQUID magnetometry measurements of the complex showed a deviation from the expected behavior for a free Eu(II) ion, which might be due to a ligand−metal interaction.

INTRODUCTION

Lanthanide complexes with the metal in the +3 oxidation state continue to dominate rare-earth chemistry.[1] The divalent oxidation state for lanthanides was first discovered for their dihalides MX_2 in the solid state,[2] and for a long time only three lanthanide elements, samarium, europium, and ytterbium, were readily accessible in the M^{2+} oxidation state. However, quite recently Evans at al. succeeded in preparing examples of all stable lanthanides in the oxidation state +2.[3,4] An explanation for this unexpected success was given by Evans, who pointed out convincingly that the reduction process Ln(III) → Ln(II) is not necessarily associated with a change in electron configuration from $4f^n \rightarrow 4f^{n+1}$ but can rather be regarded as $4f^n \rightarrow 4f^n5d^1$.[1,5] The respective $5d_{z^2}$ orbital is energetically available because of strong ligand field splitting caused by the $C_5H_4SiMe_3$ ligand. Our interest in other strong-field ligands led us to study the quite neglected area of silyl lanthanides. Recently we reported a number of lanthanide(+II) complexes bearing oligosilanyl ligands (Figure 1).[6]

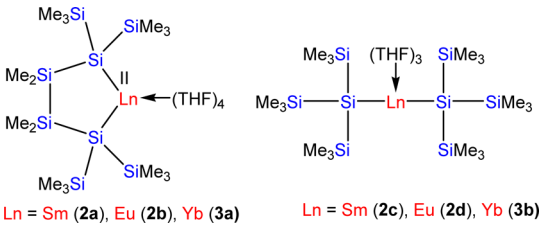

Figure 1. Oligosilanylated Ln(II) complexes.

Our first excursion into this chemistry led us to study the influence of bidentate versus monodentate silanides in their reactions with ytterbium, europium, and samarium diiodides.[6] The formation of the very air, moisture, and light sensitive compounds occurred in a facile way, and all of the neutral compounds formed shown in Figure 1 were characterized by multinuclear NMR spectroscopy and single-crystal X-ray

Received: February 15, 2017
Published: April 11, 2017

DOI: 10.1021/acs.inorgchem.7b00420
Inorg. Chem. 2017, 56, 5328−5341

Scheme 1. Synthesis of Sm(II) (2) and Yb(II) (3) Complexes with a Bidentate 1,3-Trisilanediide Ligand and Formation of Dinuclear Complex 4 by THF Loss of 2

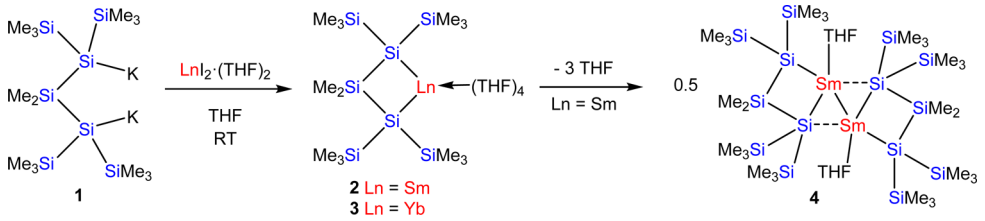

diffraction analysis. The cyclic silyl lanthanide compounds **2a,b** and **3a** contain four THF molecules, whereas the acyclic examples **2c,d** and **3b** bear only three THF molecules.[6] These coordinated solvent units do not only prevent the use of vacuum during the workup procedure but also cause a restriction to THF as a solvent in subsequent reactions in order to ensure a homogeneous product distribution with only one type of coordinated base. To overcome this limitation, we set out to find silyl frameworks that diminish solvent coordination possibilities, thus facilitating further handling and derivatization.

RESULTS AND DISCUSSION

Synthesis. Continuing the line of our previous study led us to examine reactions of the 1,3-trisilanediide $Me_2Si[Si(Me_3Si)_2K]_2$ (**1**)[7,8] with SmI_2·2THF and YbI_2·2THF, which yielded the cyclic complexes $Me_2Si[Si(Me_3Si)_2]_2Sm$·2THF (**2**) and $Me_2Si[Si(Me_3Si)_2]_2Yb$·2THF (**3**) (Scheme 1). Like the previous reactions with 1,4-tetrasilanediides, which led to the formation of five-membered rings with the lanthanide atom coordinated by four THF molecules, complexes **2** and **3**, which exist as four-membered rings, also contain the same number of coordinated THF molecules. A first attempt to crystallize samaracyclotetrasilane **2** in pentane failed but provided a few crystals of the dimeric samarium complex **4**, which were subjected to single-crystal X-ray diffraction analysis (Scheme 1). The formation of **4**, which bears only two THF units, constitutes a dimerization of **2** caused by the loss of three THF molecules from each molecule of **2**. All further efforts to selectively abstract THF molecules from **2** under defined and reproducible conditions to repeat the formation of **4** were unsuccessful.

This difficulty encouraged us to find ways of avoiding or at least diminishing coordination of THF molecules to the lanthanide. The simple idea of replacing THF by a more strongly coordinating crown ether was quickly discarded. NMR spectroscopic analysis of the addition of 18-crown-6 to the bis[tris(trimethylsilyl)silyl]ytterbium·3THF[6] complex **3b** showed just two detectable products: namely, tetrakis(trimethylsilyl)silane and tris(trimethylsilyl)silane (Scheme 2). Therefore, new silyl ligands were designed that would permit the avoidance of donor solvents, such as THF and DME, or the use of crown ethers for the preparation of the required silyl anions.

Scheme 2. Decomposition of Bis[tris(trimethylsilyl)silyl] ytterbium Complex 3b by Addition of 18-crown-6

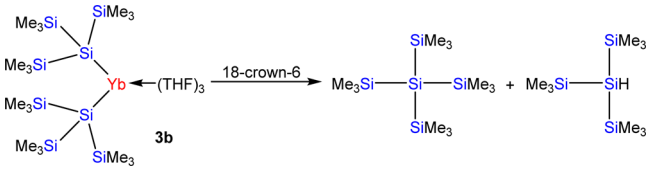

For the design of such a ligand, two possible strategies are self-evident. The first is to enhance the steric demand of the ligand to such an extent that no further space for coordinating solvent molecules is available. The second option strives to offer additional intramolecular coordination sites to the lanthanide center by incorporating donor atoms into the ligand backbone. The chosen example for a more bulky silyl ligand was pentakis(trimethylsilyl)disilanylpotassium (**5**).[9] Unfortunately, reaction of **5** with YbI_2·2THF did not proceed as expected but led to a palette of products. Upon crystallization, one of the main products, identified by X-ray crystallography, was alkoxysilylytterbium complex **6** (Scheme 3). Similar reactions involving ring-opening reactions of THF are known[10] and occur upon coordination of THF to a strongly Lewis acidic site, which renders the α-carbon electron deficient and prone to nucleophilic ring opening. In the solid state the alkoxysilylytterbium species thus formed undergoes a further dimerization step (Scheme 3). Since the steric bulk of the substituted butoxy ligand in the vicinity of the metal atom is not high enough, additional THF molecules coordinate to each of the ytterbium atoms.

The disiloxane $[(Me_3Si)_3SiSiMe_2]_2O$ (**7**) (Scheme 4) is easily accessible and was chosen to test the concept of incorporation of an oxygen atom into the silicon backbone to provide additional donor sites to the lanthanide atom. Reaction of **7** with 2 equiv of *t*-BuOK led to the formation of the respective α,ω-disilanide $[K(Me_3Si)_2SiSiMe_2]_2O$ (**8**), and in subsequent reaction steps with LnI_2·2THF (Ln = Yb, Sm) the clean formation of **9** and **10** (Scheme 4) was observed. In both compounds the lanthanide is coordinated by the two silanide atoms, three THF molecules, and the oxygen atom within the oligosilane ligand backbone.

Several other starting materials (**11**, **14**, **16**, and **17**) (Scheme 5) that might offer possibilities for intramolecular stabilization were further taken into account. α-Alkoxysilyl anions feature silylenoid behavior, making self-condensation a typical reaction.[11,12] The latter can be avoided by addition of crown ether, whereupon α-alkoxysilyl anions can be isolated. Since the presence of crown ether was found to be incompatible with silyl lanthanides, the question arose which alkoxy-substituted silyl anions could be formed without the use of crown ether.

Reaction of cyclotetrasilane **12** with *t*-BuOK was reported to give silanide **11** by a ring-opening attack on a dimethylsilylene unit.[13] Unfortunately, treatment of **11** with YbI_2·$(THF)_2$ did not result in formation of the expected Yb complex; instead, back-reaction to **12** and formation of $Yb(O^tBu)_2$ took place (Scheme 5). To find out whether the bulkiness of the *tert*-butoxy group impedes reaction of **11** with YbI_2·$(THF)_2$ to the desired lanthanide complex, compounds **14**, **16**, and **17** were chosen as starting materials bearing methoxy or methoxymethyl

DOI: 10.1021/acs.inorgchem.7b00420
Inorg. Chem. 2017, 56, 5328−5341

Scheme 3. Attempted Synthesis of Bis[pentakis(trimethylsilyl)silanyl]ytterbium Yielding Silylalkoxyytterbium Complex 6 and Other Products

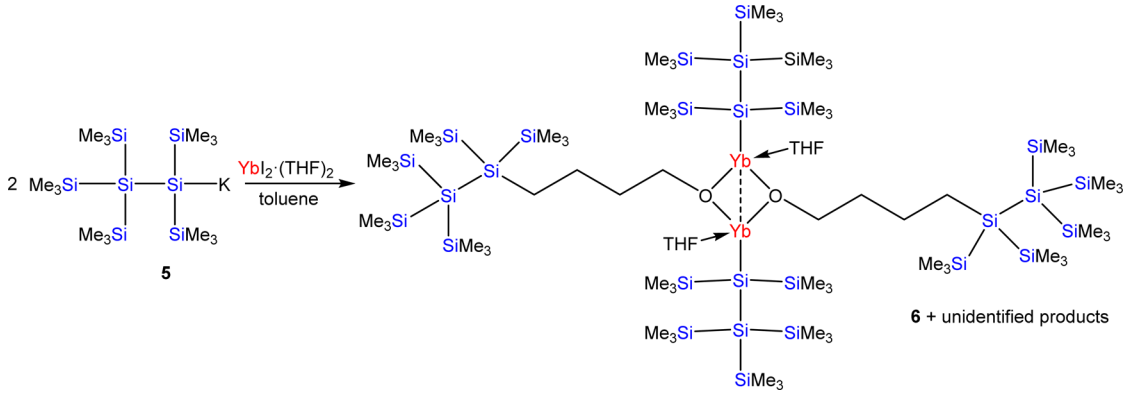

Scheme 4. Synthesis of Yb(II) (9) and Sm(II) (10) Complexes with a Tridentate Bis-Silyl Ligand

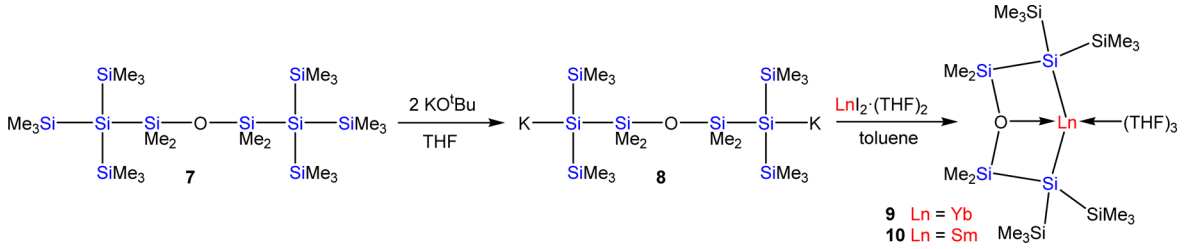

Scheme 5. Attempted Synthesis of an Yb(II) Complex with Two Bidentate 1,4-Silylalkoxy Ligands (Top Reaction) and Failed Synthetic Approaches to Other Alkoxy-Containing Silanides (Bottom Reactions)

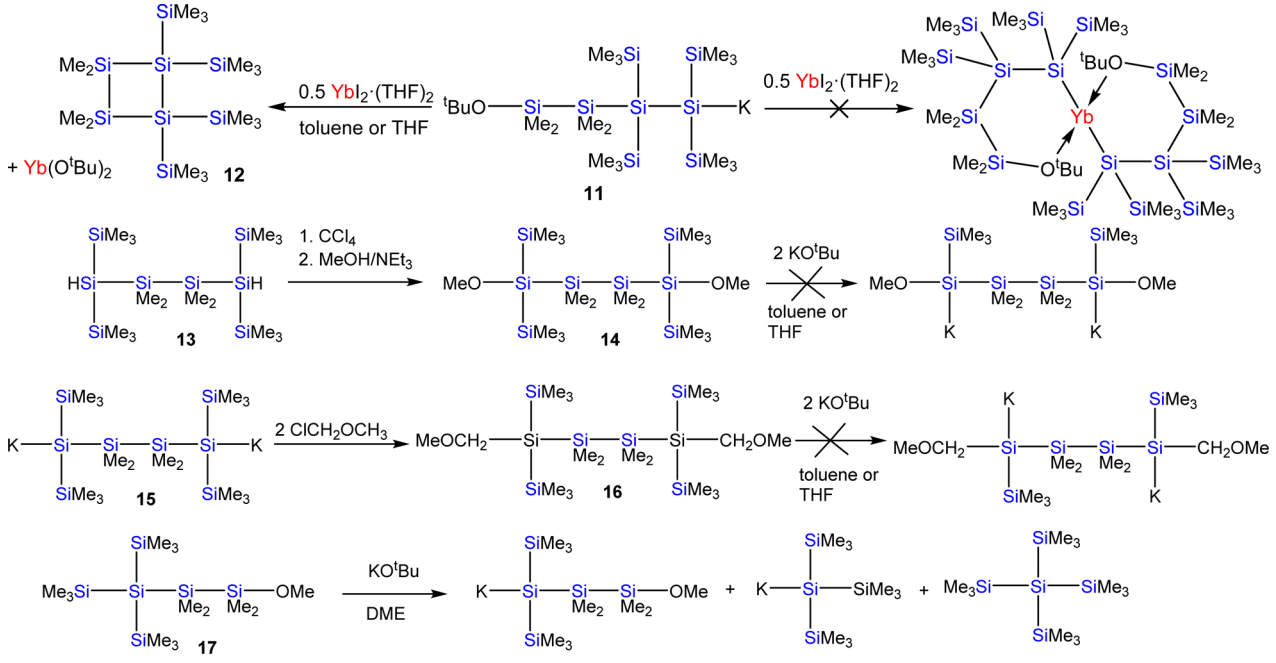

substituents (Scheme 5). Unfortunately, reactions of **14** and **16** with *t*-BuOK did not yield the respective tetrasilanediides but led to complete decomposition of both starting materials in either THF or toluene. Treatment of the methoxy compound **17** with *t*-BuOK in DME gave an inseparable mixture of the desired silyl anion together with tetrakis(trimethylsilyl)silane and tris(trimethylsilyl)silylpotassium (Scheme 5).

These problems caused us to reconsider our approach, and we decided to combine the requirements of bulkiness and a stabilizing atom in the skeleton within one silyl ligand and to put up with the disadvantage that the generation of the silyl anion has to be done in THF. In two reaction steps, ytterbium complex **19** was obtained from tris(trimethylsilyl)-methoxysilane **18**.[11] The eventual ligand, which is formed by condensation of 2 equiv of $(Me_3Si)_2Si(OMe)K$,[11] provides two coordination sites. Despite their bulkiness, the two attached ligands in **19** leave enough space at the Yb atom for the addition of one THF molecule (Scheme 6).

DOI: 10.1021/acs.inorgchem.7b00420
Inorg. Chem. 2017, 56, 5328−5341

Scheme 6. Synthesis of Yb(II) Complex 19 with Two Bidentate 1,3-Silylalkoxy Ligands

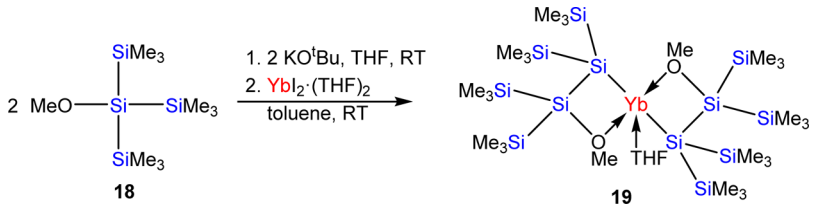

Scheme 7. Synthesis of a Bis(trimethylsilyl)silocanylsilanide and Its Subsequent Use as a Tridentate Ligand in Complexes 22 and 23

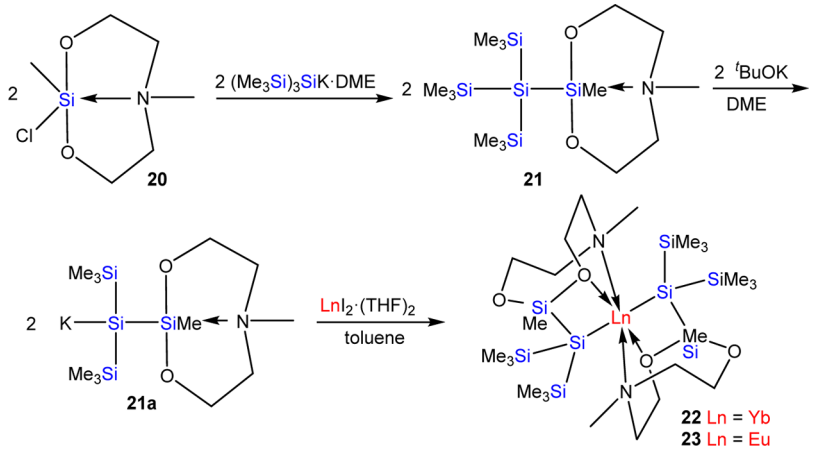

Encouraged by this result, we decided to use a simple silocane as our next ligand. Silocanes, 1,3-dioxa-6-aza-2-silacyclooctanes, contain a Si−(O−C−C−)$_2$N fragment, which we hoped would offer further coordination possibilities for the lanthanide atom. Chlorosilocane **20** (Scheme 7) was obtained by reaction of $MeSiCl_3$ with $MeN(CH_2CH_2OSiMe_3)_2$. Treatment of **20** with tris(trimethylsilyl)silylpotassium·DME afforded **21** in a clean reaction (Scheme 7). The formation of the respective oligosilocanylsilylpotassium **21a** was achieved in DME. For the next reaction steps with $LnI_2·(THF)_2$ (Ln = Yb, Eu) the solvent was exchanged for toluene. In both the Yb complex **22** and the Eu complex **23** two silocanyl units serve as ligands. The lanthanides are coordinated by the two silanides, two nitrogen atoms, and two oxygen atoms without any further solvent molecule present.

NMR Spectroscopy. In addition to the previously described disilylated Ln(II) complexes **2a,c** and **3a,b**,[6] in the current study NMR spectroscopic data of **2**, **3**, **9**, **10**, **19**, and **22** were obtained. The majority of these complexes are Yb compounds (**3a,b**, **3**, **9**, **19**, and **22**), which are diamagnetic and therefore well suited for NMR spectroscopic analysis.

^{1}H and ^{13}C NMR spectra of the Yb complexes display the expected ligand signals. All ^{1}H spectra display broadened lines indicating dynamic coordination−decoordination behavior. For complex **3** the spectra clearly show decomposition upon removal of THF.

With respect to the silyl ligand−Yb(II) interaction ^{29}Si NMR spectroscopy provides the most intimate insight. Complexes **3a,b** were found to exhibit ^{29}Si NMR signals at −158.4 and −144.8 ppm, respectively.[6] These chemical shifts indicate a silanide character of the silyl ligand. Related magnesium silanides exhibit somewhat more shielded signals,[14] whereas analogous oligosilanyl zinc compounds[15] resonate at slightly lower field. This NMR behavior is not without precedence. The tris(trimethylsilyl)silylytterbium complex $Cp^*YbSi(SiMe_3)_3·(THF)_2$, described by Lawless and co-workers,[16] showed a ^{29}Si NMR signal at −158 ppm. A signal with a similar chemical shift at −148.6 ppm was reported by Niemeyer for the ate complex $K[(Me_3Si)_3SiYb\{N(SiMe_3)_2\}_2]$.[17] Most recently Krempner and co-workers[18] described the ytterbium silanide $[Si(SiMe_2OMe)_3\text{-}\kappa^3]_2Yb$, where the interaction of the ligand with the Yb atom is only occurring via the OMe groups and no interaction between the silanide atom and the lanthanide is observed. The respective ^{29}Si NMR signal for this compound was found at −202.9 ppm. The latter value likely might be regarded as typical for a free silanide.

When the compounds of the current study are added to this analysis, the two values of −136.9 ppm and even −134.7 ppm for compounds **3** and **19**, respectively, seem to indicate a less ionic bonding situation for these cases. However, in both of these compounds the silicon atom in question is incorporated into a four-membered ring. Such an arrangement is known to cause a downfield shift of the resonances of the ring silicon atoms. The chemical shift of the magnesium analogue of **3** is at −137.3 ppm,[14] indicating a very similar polarity of the respective Si−Yb and Si−Mg bonds. The ^{29}Si chemical shift of compound **9** (−153.8 ppm) is comparable to that of **3a**, whereas the −182.0 ppm value of the silocan complex **22** are definitely rather strongly shielded into a spectroscopic range where usually potassium or lithium silanides are found.[19] This unusual shift seems to be caused by the geometry of the ligand, which by its polydentate nature forces the silanide atom to coordinate in a distorted way with diminished directionality of the silanide lone pair and the Yb atom.

For the aforementioned neutral complex $Cp^*YbSi(SiMe_3)_3·(THF)_2$ a $^1J_{Si-Yb}$ coupling constant of 829 Hz[16] was found, and for $K[(Me_3Si)_3SiYb\{N(SiMe_3)_2\}_2]$ a value of 716 Hz[17] was reported. For the acyclic complex **3b** a similar value of 732 Hz

DOI: 10.1021/acs.inorgchem.7b00420
Inorg. Chem. 2017, 56, 5328−5341

was found, and for a DME complex of **3a** a coupling of 656 Hz was reported.[6] Formation of **3a** in C_6D_6 with an approximate THF concentration of 9 equiv per Yb atom gave a ^{29}Si NMR spectrum with a diminished $^1J_{Yb-Si}$ coupling constant of 633 Hz.[6] For reasons not yet completely clear a $^1J_{Yb-Si}$ coupling constant cannot always be observed. In the current study we were only able to detect it for complex **9**, where it amounted to a value of 531 Hz. This decreased value certainly hints at a diminished bonding interaction.

Two-dimensional NMR correlation spectroscopy, in particular ^{1}H^{29}Si-gHMBC, proved to be a good tool for the assignment of signals. Especially for weakly paramagnetic complexes such as the samarium compounds **2** and **10**, this allows obtaining meaningful ^{29}Si NMR data. Using ^{1}H^{29}Si-gHMBC spectroscopy, resonances for the $SiMe_3$ groups of **2** and **10** were found at −119.3 and −118.1 ppm, respectively. The respective silanide resonances were detected at 117.9 and 117.2 ppm. The spectra did not show signals for the $SiMe_2$ units of either **2** or **10**.

As it is strongly paramagnetic, for the Eu complex **23** no meaningful NMR spectra could be obtained at all. Nevertheless, on the basis of structural data and computational results it is reasonable to state very similar bonding situations for isostructural Yb, Sm, and Eu complexes. Therefore, the results derived from NMR spectroscopic analysis of Yb complexes, which indicate a highly ionic bonding interaction between the silanide ligands and the respective Ln(II) ions, should be valid also for Sm and Eu complexes.

Crystal Structure Analysis. Samarium complex **2** crystallizes in the monoclinic space group $P2_1/c$, with four THF molecules coordinating to the Sm atom (Figure 2). Unexpectedly, the related Yb compound **3** (Figure S32 in the Supporting Information) crystallizes in the orthorhombic space group $Pna2_1$. The reason for this can be seen in Figure 3 and is a result of the different arrangement of the molecules within the crystal. In both structures, no unusual short inter- or intramolecular contacts are found. The four-membered ring in **2** is folded by 12.65° between the plane fixed by the three Si atoms and the plane fixed by Si−Sm−Si atoms. In **3** this angle is diminished to 10.75°.

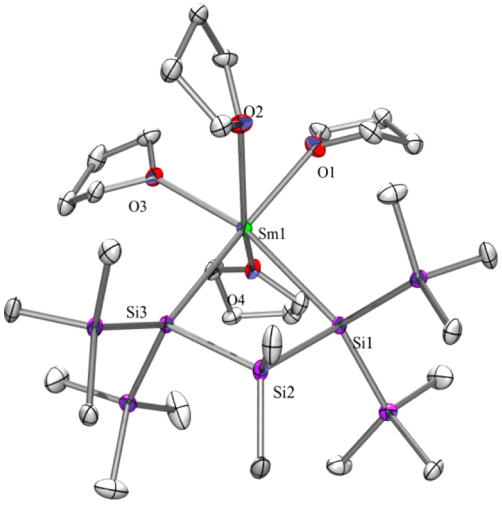

Figure 2. Molecular structure of **2** (thermal ellipsoid plot drawn at the 30% probability level). All hydrogen atoms are omitted for clarity. Selected bond lengths (Å) and angles (deg): Sm(1)−O(2) 2.561(3), Sm(1)−O(4) 2.567(3), Sm(1)−O(1) 2.587(3), Sm(1)−O(3) 2.627(2), Sm(1)−Si(3) 3.1746(11), Sm(1)−Si(1) 3.1813(11), Si(1)−Si(5) 2.3382(16), Si(1)−Si(4) 2.3397(15), Si(1)−Si(2) 2.3833(14); Si(3)−Sm(1)−Si(1) 74.66(3).

The dinuclear samarium complex **4** (Figure 4) consists of three annulated four-membered rings with the mirror plane through the central ring. This central ring is planar; the others are folded by 41.90° between the plane fixed by the three Si atoms and that fixed by Si−Sm−Si atoms.

Alkoxysilylytterbium complex **6** (Figure 5) crystallizes in the orthorhombic space group *Pbca* with an additional THF molecule in the asymmetric unit. The latter molecule is so seriously disordered that after refinement no meaningful geometry and no unambiguous atom assignment were possible; therefore, the SQUEEZE procedure[20] was applied. Several independent parts of complex **6** are disordered: namely, one trimethylsilyl group, two carbon atoms of the butylene units, and the ytterbium atoms. The four-membered ring consisting of alternate ytterbium and oxygen atoms is planar with a Yb−O bond distance of 2.246 Å (Table 1). This short Yb−O bond shows explicitly the difference between coordinated oxygen atoms of THF or the ligands and ionically bonded atoms such as in **6** (Table 1). The distance between the two Yb atoms amounts to 3.482 Å. A related dinuclear Yb(III) complex $[Cp_2YbOCH_2CH{=}CHCH_3]_2$[21] features a comparable distance of 3.536 Å.

Samarium complex **10** (Figure S34 in the Supporting Information) and the related Yb compound **9** (Figure 6) both crystallize in the monoclinic space group $P2_1/c$ with nearly identical cell parameters. The two annulated four-membered rings in **9** and **10** are only slightly bent toward each other, engaging an angle of 5.2° in **10** and 6.0° in **9**. The four-membered rings are almost planar, with one atom out of planarity by 0.334 and 0.819 Å in **10** and 0.354 and 0.849 Å in **9**.

The disiloxane **7** (Figure S33 in the Supporting Information), which serves as the starting material for **9** and **10**, crystallizes in the monoclinic space group $P2_1$. The $SiMe_2$−O−$SiMe_2$ unit and two $SiMe_3$ groups show disorder, which can be seen in the number of restraints used. The Si−O distances in **7** are 1.628 and 1.645 Å, which under the influence of the coordinating lanthanide in **9** and **10** are elongated to 1.690 and 1.697 Å.

There are more than 350 compounds in the CCDC containing at least one Sm−THF interaction, and the average Sm−O bond length is 2.51 Å. With distances between 2.50 Å for **4** and 2.63 Å for **2** (Table 1) compounds **2**, **4**, and **10** fit well into the range of observed values. The distance of the intramolecular interaction of Sm with the oxygen atom of the ligand in **10** is, at 2.588 Å, in the same range as the Sm−THF distances. Differences can be seen in the Sm−Si distances: 3.1746 and 3.1813 Å for **2**, 3.0864, 3.2010, and 3.2931 Å for **4**, and 3.183 and 3.147 Å for **10** (Table 1). These values are in good agreements with distances in our previously reported Sm(II)−silyl complexes **2a**,**c**[6] (Figure 1 and Table 1) and other reported examples.[22,23] Nevertheless, for all these compounds the bond lengths are slightly longer than the sum of the covalent radii (Sm−Si 3.09 Å).[24] Only in **4** is the distance of the tetracoordinated Si(1) to Sm(1), at 3.0864 Å, within the range of the covalent radii and is considerably shorter than those of pentacoordinated Si(3) to Sm(1a) at 3.2010 Å and Si(3a) to Sm(1) at 3.2931 Å. The complexes known in the literature with divalent samarium are mainly mononuclear, and only a few dinuclear complexes have been reported so far.[25]

DOI: 10.1021/acs.inorgchem.7b00420
Inorg. Chem. 2017, 56, 5328−5341

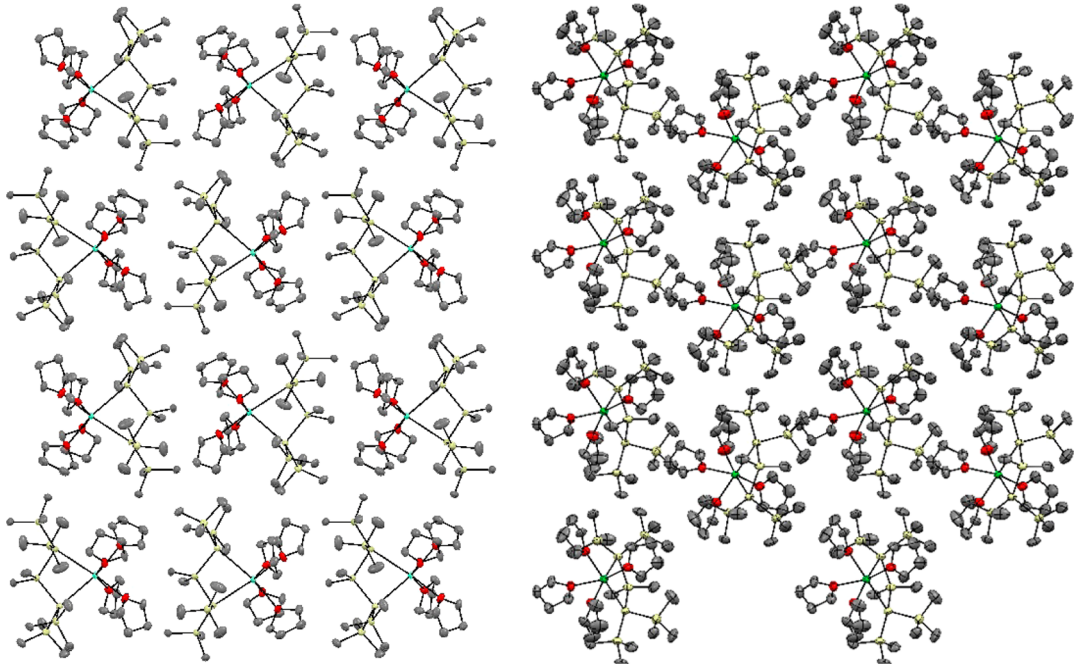

Figure 3. (left) Packing of Sm compound **2** along the *a* axis. (right) Packing of Yb compound **3** along the *b* axis.

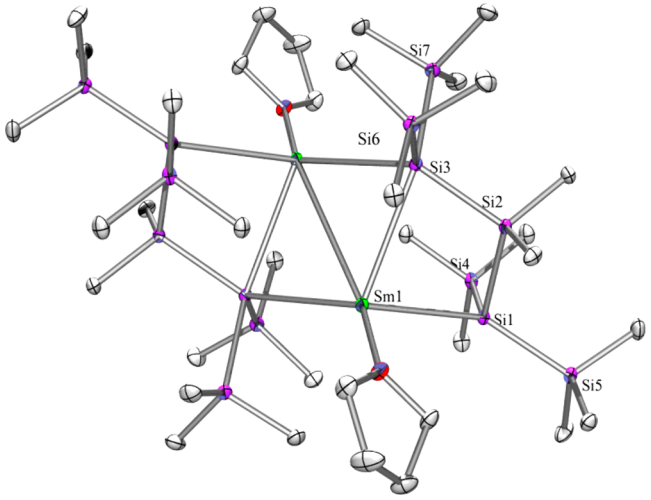

Figure 4. Molecular structure of **4** (thermal ellipsoid plot drawn at the 30% probability level). All hydrogen atoms are omitted for clarity. Selected bond lengths (Å) and angles (deg): Sm(1)−O(1) 2.5044(15), Sm(1)−Si(1) 3.0864(8), Sm(1)−Si(3) 3.2010(8), Sm(1)−Si(3a) 3.2931(7), Sm(1)−Sm(1a) 3.8898(9), Si(1)−Si(4) 2.3306(8), Si(1)−Si(5) 2.3413(8), Si(1)−Si(2) 2.3604(10), Si(2)−C(2) 1.891(2), Si(2)−C(1) 1.906(2), Si(2)−Si(3) 2.3963(8), Si(3)−Si(6) 2.3555(10), Si(3)−Si(7) 2.3601(9); Si(1)−Sm(1)−Si(3) 76.428(18), Si(1)−Sm(1)−Sm(1a) 104.330(12), Si(3)−Sm(1)−Sm-(1a) 54.297(16), Si(3a)−Sm(1)−Sm(1a) 52.126(17), Si(4)−Si(1)−Sm(1) 107.25(2), Si(5)−Si(1)−Sm(1) 143.14(3), Si(2)−Si(1)−Sm(1) 81.72(2), Sm(1)−Si(3)−Sm(1a) 73.58(2).

The Sm−Sm distance varies from within the bonding range of 3.3159 Å[25] or 3.552 Å[26] up to 4.195 Å,[27−30] far from a bonding distance considering the Sm−Sm atom distances in the metal being 3.588 and 3.620 Å.[31] In complex **4** a Sm−Sm distance of 3.8898 Å was found and some interaction might be possible.

Spirocyclic ytterbium compound **19** crystallizes in the triclinic space group $P\bar{1}$ (Figure 7). The two four-membered rings are almost planar with Si(7) 0.311 Å and Si(1) 0.334 Å out of planarity. Further, the two rings are engaging an angle of 142.7° and thus provide space for the additional THF molecule.

Silocanyl chloride **20** (Figure S35 in the Supporting Information) crystallizes in the monoclinic space group $P2_1/n$. The Si−N distance in **20** is 2.117 Å and thus is essentially longer than the 2.023 Å in a related chlorosilatrane.[32] Nevertheless, this distance is within the range (2.0−2.2 Å) of a transannular interaction between Si and N.[33] No interaction between Si and N is observed in **22** (Figure S36 in the Supporting Information) and **23** (Figure 8), where the Si−N distance is 3.711 Å for **22** and 3.709 Å for **23** due to the influence of the Ln−N coordination. Both Ln−Si complexes crystallize in monoclinic space groups, **22** in *C*2 and **23** in *C*2/*c*. Here again, as was mentioned for **2** and **3**, the differences in the cell parameters arise from the arrangement within the crystal packing (Figure S37 in the Supporting Information). Only a couple of structures bearing Yb(II)−Si bonds can be found in the literature,[6,16,17,34−37] but these distances are in good agreement with those found for **3**, **9**, **19**, and **22** (Table 1). For Eu(II)−Si only three examples can be found and again distances of compound **23** compare well to these.[6,37]

Theoretical Studies. The electronic structures of **2** and **4** were calculated at the B3PW91/Basis1 level of theory. Previously we proved that this methodology yielded an adequate description of the electronic structure of f-*block*-silyl complexes.[38] Table 2 contains the calculated average Sm−Si bond lengths (Å), Mayer bond order (MBO) of Sm−Si bonds, Natural Population Analysis charges, and HOMO energies (eV) for **2** and **4**. We found excellent agreement between computed and measured bond lengths (see Tables 1 and 2), which confirmed again that our chosen method is appropriate. The electronic structures of **2** and **4** are similar to each other in the sense that all samarium centers have six−six unpaired f electrons ($S = 3$) in all complexes while the silyl groups bear an additional electron, best described as silyl anions. Compound **4**, the dimerization product of **2**, contains two samarium centers 3.90 Å from each other. We found that the ground state is a

DOI: 10.1021/acs.inorgchem.7b00420
Inorg. Chem. 2017, 56, 5328−5341

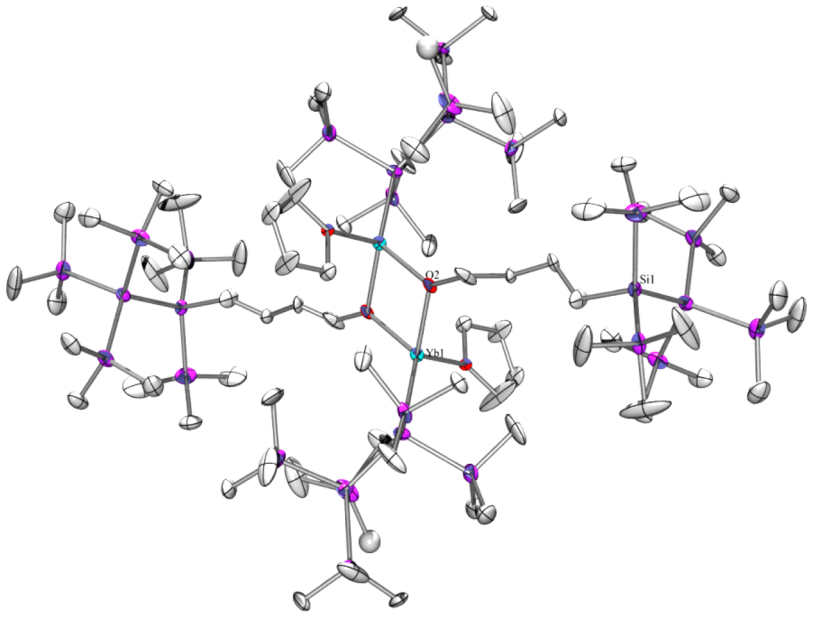

Figure 5. Molecular structure of **6** (thermal ellipsoid plot drawn at the 30% probability level). All hydrogen atoms are omitted for clarity. Selected bond lengths (Å) and angles (deg): Yb(1)−O(1) 2.371(8), Yb(1)−O(2) 2.248(5), Yb(1)−Si(1) 3.015(3), Yb(1)-Yb(1A) 3.4825(9), Si(1)−Si(2) 2.322(3), Si(1)−Si(4) 2.381(3), Si(2)−C(1) 1.848(8); O(2)−Yb(1)−Si(1) 118.67(18), O(1)−Yb(1)−C(36) 80.6(3).

Table 1. Compilation of Structural Data Derived by Single-Crystal XRD Analysis of Complexes 2−4, 6, 9, 10, 19, 22, and 23 and the Related Compounds 2a−d and 3a,b

Si−Sm (Å)	Sm−O (Å)	Si−Yb (Å)	Yb−O (Å)	Yb−N (Å)	Si−Eu (Å)	Eu−O (Å)	Eu−N (Å)
2: 3.175, 3.181	**2**: THF, 2.561− 2.627	**3**: 3.057, 3.066	**3**: THF, 2.437−2.492				
2a:[6] 3.213, 3.244	**2a**:[6] THF, 2.544− 2.613	**3a**:[6] 3.106, 3.171	**3a**:[6] THF, 2.433−2.485		**2b**:[6] 3.205, 3.216	**2b**:[6] THF, 2.546−2.613	
2c:[6] 3.172	**2c**:[6] THF, 2.551− 2.528	**3b**:[6] 3.064	**3b**:[6] THF, 2.421−2.435		**2d**:[6] 3.150	**2d**:[6] THF, 2.515-2.524	
4: 3.086, 3.201 3.293	**4**: THF, 2.504	**6**: 3.015	**6**: THF, 2.371; ionic, 2.248				
10: 3.183, 3.147	**10**: THF, 2.558−2.568; intra, 2.588	**9**: 3.053, 3.086	**9**: THF, 2.434−2.460; intra, 2.471				
		19: 3.047, 3.063	**19**: THF, 2.364; intra, 2.365, 2.377				
		22: 3.050	**22**: intra, 2.491	**22**: 2.705	**23**: 3.157	**23**: intra, 2.602	**23**: 2.765

high-spin system (S = 6); no lower energy broken-symmetry states were found. This suggests that the samarium centers have direct exchange interaction in spite of the relatively large distance.

The Si−Sm bond lengths in **2** and **4** (3.17−3.20 Å) are longer than those of our previously characterized relatively covalent f-*block*-silyl structures[6,38] that also suggest strong ionic character. Natural population analysis (NPA) also revealed strong ionic character of Sm−Si bonds; silicon atoms possess almost a clear extra electron (Table 2), as NPA charges ranged between −0.72 and −0.80, while samarium centers have large positive charge. Mayer bond orders (MBO) are relatively low (~0.3), similar to the case for our previous Sm−silylene complexes,[38] which also indicates negligible covalent character. HOMO orbitals underline this analysis (Figures 9 and 10), as they resemble lone pairs situated on silicon centers with no extension toward the samarium centers.

We also calculated the electronic structure of **23** at the B3PW91/Basis1 level of theory as for the previous f-block complexes. Complex **23** was found to possess seven unpaired electrons (S = 7/2), all occupying f orbitals. These singly occupied molecular orbitals (SOMOs) are very close in energy to each other in the range of −2.60 to −3.31 eV. Interestingly, very close to the unpaired f electrons in energy there are two doubly occupied molecular orbitals (formally denoted as the HOMO of **23**, Table 2) of the silicon lone pairs, −3.75 and −3.44 eV, respectively. This small energy difference between the lowest lying SOMO and HOMO might be one reason for the peculiar magnetism of **23**. Finite temperature effects or crystal-packing effects can overcome the only 0.12 eV difference, and the error of DFT can be very large in strong correlation problems. Nevertheless, none of our efforts using other DFT functionals resulted in a ground state solution that could explain the magnetic properties of **23**.

HOMO orbitals show very clear silyl anion character (Figure 11), which is in agreement with the very large NPA negative charge (−0.88) on the silicon centers that is even larger than those of **2** and **4**. Together with very low Mayer bond order values (0.25), these results all indicate the highest ionic character that we have observed in our f-block silyl complexes that can explain the very high energy of the silyl anion orbitals close to the f orbitals.

DOI: 10.1021/acs.inorgchem.7b00420
Inorg. Chem. 2017, 56, 5328−5341

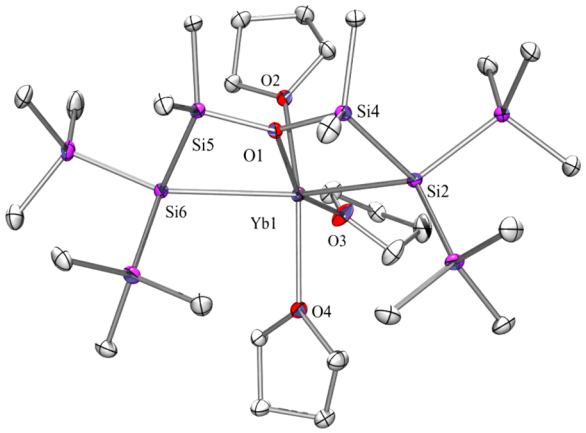

Figure 6. Molecular structure of **9** (thermal ellipsoid plot drawn at the 30% probability level). All hydrogen atoms are omitted for clarity. Selected bond lengths (Å) and angles (deg): Yb(1)−O(2) 2.4350(16), Yb(1)−O(4) 2.4354(17), Yb(1)−O(3) 2.4598(18), Yb(1)−O(1) 2.4707(15), Yb(1)−Si(2) 3.0528(9), Yb(1)−Si(6) 3.0860(8), Si(1)−C(1) 1.889(3), Si(1)−Si(2) 2.3415(10); O(2)−Yb(1)−O(1) 86.87(6), O(4)−Yb(1)−O(1) 124.26(6), O(3)−Yb(1)−O(1) 156.64(6), O(1)−Yb(1)−Si(2) 68.98(4), O(1)−Yb(1)−Si(6) 68.60(4), Si(2)−Yb(1)−Si(6) 133.95(2), O(1)−Yb(1)−Si(5) 28.34(4), Si(2)−Yb(1)−Si(5) 97.318(18), Si(6)−Yb(1)−Si(5) 41.987(16), Si(2)−Yb(1)−Si(4) 41.760(16), Si(6)−Yb(1)−Si(4) 95.64(2), Si(5)−Yb(1)−Si(4) 55.770(19).

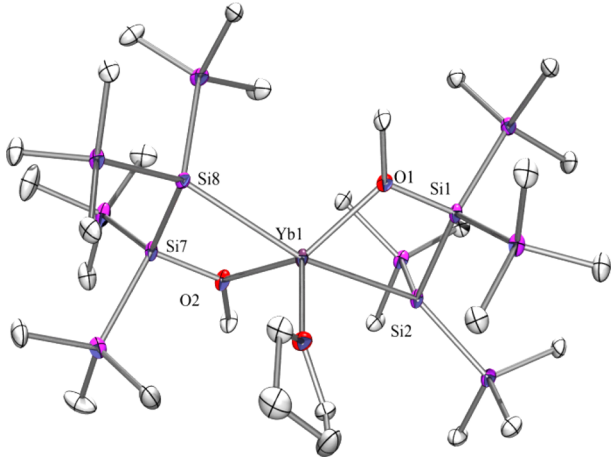

Figure 7. Molecular structure of **19** (thermal ellipsoid plot drawn at the 30% probability level). All hydrogen atoms are omitted for clarity. Selected bond lengths (Å) and angles (deg): Yb(1)−O(3) 2.364(4), Yb(1)−O(1) 2.365(4), Yb(1)−O(2) 2.377(4), Yb(1)−Si(8) 3.0469(17), Yb(1)−Si(2) 3.0627(17), Si(1)−O(1) 1.750(4), Si(1)−Si(2) 2.361(2), Si(3)−C(5) 1.863(7), Si(7)−O(2) 1.749(4); O(1)−Yb(1)−O(2) 143.23(14), O(1)−Yb(1)−Si(8) 104.42(10), O(2)−Yb(1)−Si(8) 68.59(10), O(1)−Yb(1)−Si(2) 69.05(9), O(2)−Yb(1)−Si(2) 105.62(10), Si(8)−Yb(1)−Si(2) 161.35(5), O(1)−Yb(1)−Si(1) 27.85(9), O(2)−Yb(1)−Si(1) 139.25(10), Si(8)−Yb(1)−Si(1) 132.05(4), Si(2)−Yb(1)−Si(1) 42.01(4), O(1)−Yb(1)−Si(7) 137.95(10), O(2)−Yb(1)−Si(7) 27.55(9), Si(8)−Yb(1)−Si(7) 41.75(4), Si(2)−Yb(1)−Si(7) 132.86(4), Si(1)−Yb(1)−Si(7) 155.22(4).

SQUID Magnetometry on Silocane−Eu Complex 23.

Among the rare-earth elements, europium in the valence state Eu(II) plays an exceptional role due to the compensation of orbital momentum ($L = 0$) in the free-ion state $^8S_{7/2}$ providing the utmost spin momentum of seven unpaired spins ($S = 7/2$).

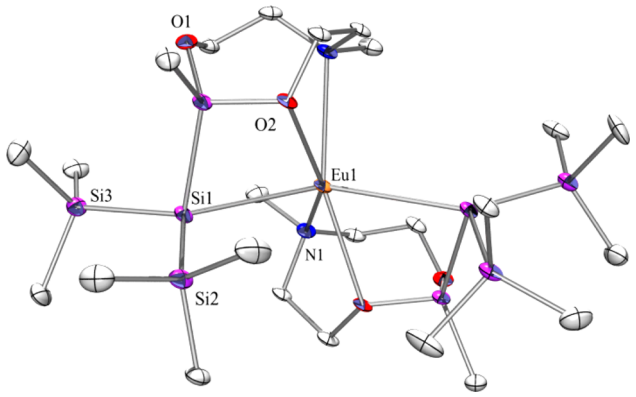

Figure 8. Molecular structure of **23** (thermal ellipsoid plot drawn at the 30% probability level). All hydrogen atoms are omitted for clarity. Selected bond lengths (Å) and angles (deg): Eu(1)−O(2) 2.602(4), Eu(1)−N(1) 2.765(5), Eu(1)−Si(1) 3.157(2), Si(1)−Si(2) 2.342(3), Si(4)−O(1) 1.659(5), Si(4)−O(2) 1.721(5), Si(2)−C(1) 1.881(7); O(2)−Eu(1)−O(2A) 143.80(19), O(2)−Eu(1)−N(1) 148.91(14), O(2)−Eu(1)−Si(1) 65.43(10), N(1)−Eu(1)−Si(1) 99.05(12), Si(1)−Eu(1)−Si(4A) 129.10(5), O(2)−Eu(1)−Si(4) 28.28(10), N(1)−Eu(1)−Si(4) 124.82(11).

Table 2. Calculated Average Ln−Si Bond Lengths (Å), Mayer Bond Order (MBO) of Ln−Si Bonds, Natural Population Analysis Charges, and HOMO Energies (eV) for 2, 4, and 23 at the B3PW91/Basis1 Level of theory

compound	Sm−Si bond distance (Å)	MBO of Sm−Si bond	NPA charge (Sm/Si)	HOMO energy (eV)
2	3.180	0.36	+1.37/−0.74	−3.11
4	3.080	0.61	+1.25/−0.80	
	3.204	0.35	−0.72	−3.82
	3.297	0.21		
23	3.157	0.25	+1.64/−0.88	−3.44
	3.493	0.04		

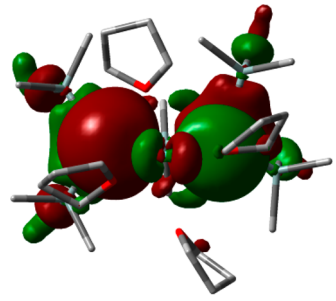

Figure 9. HOMO orbital of **2** (−3.48 eV), calculated at the B3PW91/Basis1 level of theory (isovalue 0.02). White, gray, blue, red, and teal colors refer to hydrogen, carbon, oxygen, samarium, and silicon atoms, respectively.

The absence of orbital momentum makes Eu(II) unsusceptible to spin−orbit coupling and diminishes ligand field effects. The first excited state ($^6P_{7/2}$) is located at some 30.000 cm^{-1} above the ground state energy.[39] Therefore, at ambient temperature only the ground state becomes mainly populated, and its zero-field splitting is very weak, on the order of 10^{-2} cm^{-1}, only detectable in the temperature range of sub-Kelvin. From these findings of the free-ion Eu(II) state the magnetic susceptibility is almost perfectly isotropic and follows the paramagnetic Curie law for $S = 7/2$ (Landé g factor equal to 2) (eq 1).

DOI: 10.1021/acs.inorgchem.7b00420
Inorg. Chem. 2017, 56, 5328−5341

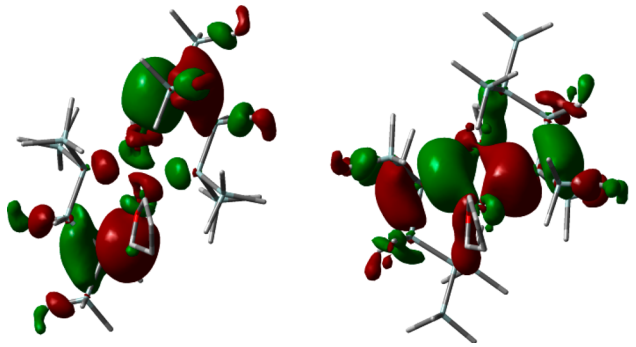

Figure 10. HOMO (left, −3.82 eV) and HOMO-2 (right, −4.65 eV) orbitals of **4** calculated at the B3PW91/Basis1 level of theory (isovalue 0.02). White, gray, blue, red, and teal colors refer to hydrogen, carbon, oxygen, samarium, and silicon atoms, respectively.

$$\chi_{mol}(T) = \frac{N_A g^2 \mu_B^2 S(S+1)}{3k_B T} = \frac{7.88\ [\mathrm{cm^3\ K\ mol^{-1}}]}{T\ [\mathrm{K}]} \quad (1)$$

The fundamental constants are Avogadro's number N_A = 6.022 × 10^{23}/mol, Bohr magneton μ_B = 9.274 × 10^{-21} emu, and Boltzmann's constant k_B = 1.38 × 10^{-23} J/K. The Curie law holds for small magnetic fields and high temperatures. We measured the Curie constant $\chi_{mol}T$ [cm^3 K mol^{-1}] of the silocane−Eu compound **23** at very high magnetic fields (B = 1, 7 T) down to low temperatures $T \rightarrow$ 2.7 K, for which the Curie law has to be modified, as shown in eq 2

$$\chi_{mol}T = \frac{N_A g \mu_B S B_S(g\mu_B S B/k_B T)}{B} \quad (2)$$

where $B_S(x)$ is the Brillouin-function for spin S as depicted in eq 3.

$$B_S(x) = \frac{2S+1}{2S}\coth\left(\frac{2S+1}{2S}x\right) - \frac{1}{2S}\coth\frac{x}{2S} \quad (3)$$

The top blue solid line in Figure 12a displays the calculated $\chi_{mol}T$ according to eq 2 as a function of temperature for B = 1 T. Clearly, this curve approaches the high-temperature value 7.88 cm^3K mol^{-1} as calculated by eq 1. It shows the characteristic turn-down at low temperature due to saturation. Interestingly, the measured molar Curie constant of the Eu complex **23** (blue crosses of Figure 12) exhibits a deviation from the curvature at low temperature T < 100 K. This deviation from the free-ion magnetic state becomes less pronounced for higher magnetic field (7 T), as shown by the red graphs of Figure 12a. Figure 12b shows an enlarged view in the temperature range 20−100 K.

As mentioned already, the ground state level of isolated Eu(II) is not split. However, in the silocane−Eu complex **23** the influence of ligands and of crystallinity could change the situation. It is out of the scope of this paper to recover these effects or the influence of a possible charge transfer.

Figure 13 shows the field-dependent molar magnetization for four temperatures (T = 2.7, 6, 10, 20 K). The fits (solid lines) approximate the measured data (dots) only if 88% of Eu is in the "pure" S = 7/2 spin state, what again implicates that not all Eu ions can be represented by "free" ions.

As a result of the magnetic measurements we conclude that an anticipated (S = 7/2) state of seven unpaired and unsplit (zero-field) spin states in Eu(II) is superficial but does not explain in detail the experimental data in complex **23** at reduced temperatures. DFT data (vide supra) suggest a moderate splitting of 0.12 eV between SOMO and HOMO molecular orbitals with a corresponding influence on the Eu spin state. In any case, all the Eu atoms cannot be in the S = 7/2 pure spin states, as demonstrated.

CONCLUSION

The current work continues the study of silylated lanthanides. Reaction of a potassium 1,3-trisilandiide with SmI_2 and YbI_2 was found to give disilylated complexes of samarium (**2**) and ytterbium (**3**). As the bite angle of the oligosilanediyl ligand is small, four THF molecules coordinate to the Ln(II) metal atoms. Dissociation of THF is a facile process, complicating isolation of homogeneous substances. In the case of samarium complex **3** it was possible to isolate the defined dimerization product **4**, which is a dinuclear complex where dissociated THF molecules are replaced by the silanide units of the neighboring complex.

To facilitate isolation and handling of silyl lanthanide complexes, we set out to modify the silyl ligands' coordinative properties by incorporating additional donor atoms which serve as Lewis basic sites. Using this approach, it was possible to diminish the coordinating THF molecules to one or even none. While the obtained complexes are still very sensitive toward light and ambient conditions, the ligand modifications diminish the chance of dissociation of coordinated solvent molecules and thus increase the stability of the complex.

Due to the paramagnetism of unpaired f electrons, NMR spectroscopy of lanthanide complexes is frequently difficult. Diamagnetic Yb(II) complexes with a completely filled f shell are an exception to this and provide valuable insight into the electronic properties. ^{29}Si NMR spectroscopic analysis of the Yb−silyl complexes studied in this work reemphasizes the already previously gained insight that the nature of the Si−Ln bond in these complexes is highly ionic. The strongly downfield shifted resonances of the metal-attached silicon atoms indicate high silanide character. This is particularly true for the Yb

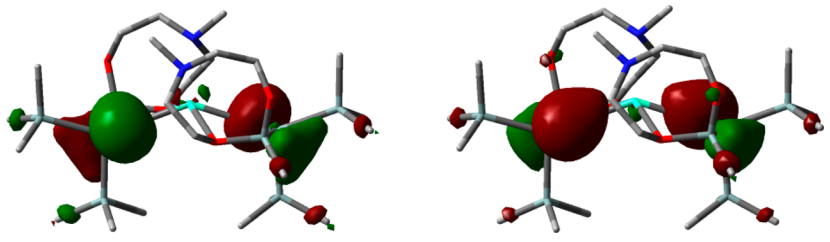

Figure 11. HOMO (left, −3.44 eV) and HOMO-2 (right, −3.75 eV) orbitals of **23** calculated at the B3PW91/Basis1 level of theory (isovalue 0.02). White, gray, blue, red, and teal colors refer to hydrogen, carbon, oxygen, samarium, and silicon atoms, respectively.

DOI: 10.1021/acs.inorgchem.7b00420
Inorg. Chem. 2017, 56, 5328−5341

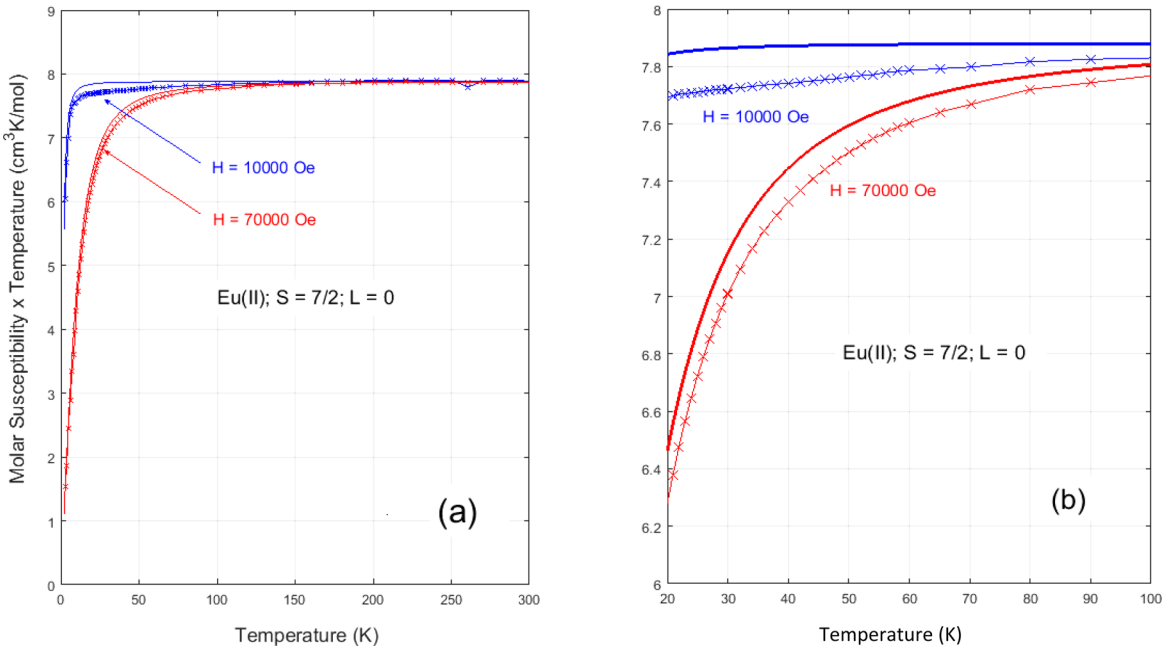

Figure 12. Calculated molar Curie constants $\chi_{mol}T$ of the "free ion" Eu(II), in comparison with SQUID measurements of **23** (marked as crosses) represented by the blue graphs (for $B = \mu_0 H = 1$ T) and by the red graphs (for $B = \mu_0 H = 7$ T): (a) the common Curie constant of 7.88 cm^3 K mol^{-1} in the limit at high temperature (300 K); (b) detailed view in the reduced temperature range of 20−100 K, in which the measurement deviates from the free-ion $S = 7/2$ spin state.

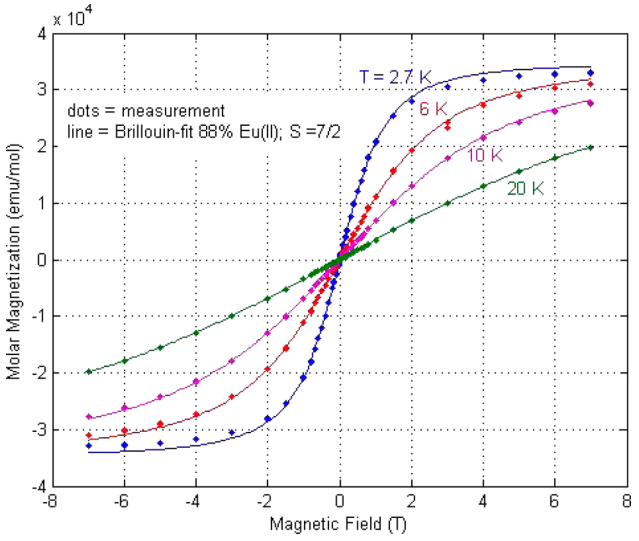

Figure 13. Isothermal magnetization curves of Eu complex **23** for various temperatures. The measured data (dots) are best fitted (solid lines) by 88% of the "pure" 7/2 spin magnetization of Eu(II).

complex with the bis(trimethylsilyl)silocanylsilyl ligand, for which a chemical shift of −182.0 ppm was observed.

The NMR analysis was supported by DFT calculations, which show that the HOMOs of the complexes consist mainly of silicon lone pairs without extension toward the lanthanide centers. According to natural population analysis (NPA) the silicon atoms possess almost a clear extra electron while the lanthanide centers have a large positive charge. In addition, the Mayer bond orders (MBOs) are relatively low (∼0.3). Calculation of the electronic structure of europium complex **23** confirmed the expected half-filled shell of seven unpaired electrons ($S = 3/2$). It is interesting to note that these singly occupied molecular orbitals (SOMOs), which are very close in energy to each other in the range of −2.60 to −3.31 eV, are also very close to the two doubly occupied molecular orbitals (HOMOs) of the silicon lone pairs, −3.75 and −3.44 eV, respectively.

With its seven unpaired electrons europium(II) complex **23** is also interesting with respect to its magnetic properties. Using SQUID magnetometry measurements the Curie constant $\chi_{mol}T$ [cm^3 K mol^{-1}] of **23** at very high magnetic fields (B = 1, 7 T) down to low temperatures $T \rightarrow 2.7$ K was determined. Interestingly, molar Curie constants χ_{mol} of the "free" Eu(II) ion, in comparison with the SQUID measurements of **23** show that in a plot of χ_{mol} vs T the observed curve approaches the expected high temperature value of 7.88 cm^3 K mol^{-1}. However, the measured molar Curie constant of **23** shows a deviation from the expected curvature at low temperature $T <$ 100 K which becomes less pronounced for higher magnetic field (7 T). The origin of this behavior is not yet clear but may be caused by the close proximity of the lowest SOMO and the HOMO of **23**.

EXPERIMENTAL SECTION

General Remarks. All reactions involving air-sensitive compounds were carried out under an atmosphere of dry nitrogen or argon using either Schlenk techniques or a glovebox. All solvents were dried using a column-based solvent purification system.[40] 1,3-Dichloro-1,1,3,3-tetramethyldisiloxane, $MeSiCl_3$, and other chemicals used were obtained from different suppliers and used without further purification. K-$(Me_3Si)_2$Si-$SiMe_2$-Si$(SiMe_3)_2$-K (**1**),[7,8] $(Me_3Si)_3$Si-$(Me_3Si)_2$Si-K (**5**),[9] ^{t}BuO$(Me_2Si)_2$-$(Me_3Si)_2$Si-$(Me_3Si)_2$Si-K (**11**),[13] $(Me_3Si)_2$SiH-$(SiMe_2)_2$-SiH$(SiMe_3)_2$ (**13**),[8] K-$(Me_3Si)_2$Si-$(SiMe_2)_2$-Si$(SiMe_3)_2$-K (**15**),[8] $(Me_3Si)_3SiOMe$ (**18**),[11] $MeN(CH_2CH_2OSiMe_3)_2$,[41] $(Me_3Si)_3$Si-Me_2Si-$SiMe_2$Cl,[42] and $(Me_3Si)_3SiK$[9] were prepared following reported procedures. SmI_2·2THF, YbI_2·2THF, and EuI_2·2THF were prepared by treatment of the metals in THF with 1,2-diiodoethane.[43−45]

^{1}H (300 MHz), ^{13}C (75.4 MHz), and ^{29}Si (59.3 MHz) NMR spectra were recorded on a Varian INOVA 300 spectrometer. If not

DOI: 10.1021/acs.inorgchem.7b00420
Inorg. Chem. 2017, 56, 5328−5341

noted otherwise, all samples were measured in C_6D_6. To compensate for the low isotopic abundance of ^{29}Si, the INEPT pulse sequence was used for the amplification of the signal.[46,47] Elementary analyses were carried out using a Heraeus VARIO ELEMENTAR instrument.

X-ray Structure Determination. For X-ray structure analyses the crystals were mounted onto the tip of glass fibers, and data collection was performed with a BRUKER-AXS SMART APEX CCD diffractometer using graphite-monochromated Mo Kα radiation (0.71073 Å). The data were reduced to F_o^2 and corrected for absorption effects with SAINT[48] and SADABS,[49,50] respectively. The structures were solved by direct methods and refined by full-matrix least-squares methods (SHELXL97).[51] If not noted otherwise, all non-hydrogen atoms were refined with anisotropic displacement parameters. All hydrogen atoms were located in calculated positions to correspond to standard bond lengths and angles. Crystallographic data (excluding structure factors) for the structures of compounds **2**–**4**, **6**, **7**, **9**, **10**, **19**, **20**, **22**, and **23** reported in this paper have been deposited with the Cambridge Crystallographic Data Center as supplementary publication nos. CCDC 1026160 (**2**), 1509714 (**3**), 1026161 (**4**), 1526976 (**6**), 1509720 (**7**), 1509719 (**9**), 1509718 (**10**), 1509716 (**19**), 1509721 (**20**), 1509715 (**22**), and 1509717 (**23**). Copies of data can be obtained free of charge at http://www.ccdc.cam.ac.uk/products/csd/request/. Figures of solid-state molecular structures were generated using Ortep-3 as implemented in WINGX[52] and rendered using POV-Ray 3.6.[53]

$Me_2Si[Si(Me_3Si)_2]_2Sm{\cdot}2THF$ (2). To a solution of $SmI_2{\cdot}2THF$ (288 mg, 0.525 mmol) in THF (10 mL) was added freshly prepared silanide **1** (0.500 mmol) in THF (8 mL) dropwise. The addition went along with a color change to dark green and formation of a gray precipitate. The mixture was stirred for 3 h followed by concentration of the volume to 1 mL under reduced pressure. The dark green residue was extracted with toluene (5 × 4 mL). The extract was concentrated to 15 mL and stored at −35 °C for 3 days, affording green crystals of **2** (192 mg, 45%). Mp: 167−169 °C. ^1H NMR (δ in ppm): 3.17 (s, 16H, THF), 1.34 (bs, 36H, $SiMe_3$), 0.30 (s, 16H, THF), −1.16 (s, 4H, $SiMe_2$). ^{13}C NMR (δ in ppm): 119.4 (THF), 25.0 (THF), $SiMe_2$ and $SiMe_3$ signals not detected. ^{29}Si NMR (δ in ppm): no signals detected. ^1H NMR (δ in ppm, d_8-THF): 3.58 (s, 16H, THF), 1.69 (s, 16H, THF), −0.12 (s, 36H, $SiMe_3$), −1.07 (s, 6H, $SiMe_2$). ^{13}C NMR (δ in ppm, d_8-THF): 70.6 (THF), 26.8 (THF), 23.4 ($SiMe_2$), −18.1 ($SiMe_3$). ^{29}Si NMR (δ in ppm, d_8-THF): 117.9 (Si_q), $SiMe_2$ not detected, −119.3 ($SiMe_3$). Anal. Calcd for $C_{30}H_{74}O_4Si_7Sm$ [846.32]: C, 42.60; H, 8.82. Found: C, 42.38; H, 8.37. UV absorption: λ_1 242 nm ($\varepsilon_1 = 3.5 \times 10^4$ M^{-1} cm^{-1}).

$Me_2Si[Si(Me_3Si)_2]_2Yb{\cdot}2THF$ (3). To a solution of $YbI_2{\cdot}(THF)_2$ (83 mg, 0.14 mmol) in toluene (4 mL) was added freshly prepared silanide **1** (0.14 mmol) in toluene (8 mL) dropwise under strict exclusion of light. The addition went along with a color change to orange. The mixture was stirred for 15 min, after which the solvent was removed. The residue was extracted with pentane (3 × 2 mL) and the extract filtered over Celite. The solvent was reduced to a volume of 2 mL, and a gray precipitate emerged which was dissolved by adding a few drops of THF. This solution was stored for 1 week at −37 °C, affording red crystals of **3** (47 mg, 37%). Mp: 139−140 °C. ^1H NMR (δ in ppm): 3.73 (bs, THF), 1.58 (bs, THF), 1.17 0.59 (s, 6H, $SiMe_2$), 0.74 (s, 36H, $SiMe_3$). ^{13}C NMR (δ in ppm): 68.2 (THF), 25.6 (THF), 7.9 ($SiMe_3$), 3.2 ($SiMe_2$). ^{29}Si NMR (δ in ppm): −4.6 ($^2J_{Yb-Si}$ = 19.4 Hz, $SiMe_3$), −32.7 ($SiMe_2$), −136.9 (Si_q).

Dinuclear Samarium Complex 4. Crystalline **2** (10 mg) was dissolved in pentane. Crystals suitable for X-ray analysis formed after several weeks at room temperature. Mp: 170−173 °C.

Reaction of Pentakis(trimethylsilyl)disilanylpotassium (5) with $YbI_2{\cdot}(THF)_2$. To a solution of $YbI_2{\cdot}(THF)_2$ (98 mg, 0.17 mmol) in toluene (2 mL) was added freshly prepared silanide **5** in toluene (4 mL) dropwise under strict exclusion of light. (**5** was obtained from hexakis(trimethylsilyl)silane (170 mg, 0.34 mmol) and KO^{t}Bu (40 mg, 0.36 mmol) in THF (1 mL). After complete conversion THF was removed and replaced by toluene.) Further treatment was as reported for **3**. After crystallization for 2 weeks at −37 °C out of pentane a few crystals of **6** (mp: 233−234 °C) were obtained. NMR measurements showed a number of different unidentified products.

1,3-Bis[tris(trimethylsilyl)silyl]-1,1,3,3-tetramethyldisiloxane (7). To a solution of 1,3-dichlorotetramethyldisiloxane (10.5 g, 51.7 mmol) in toluene (250 mL) were added tris(trimethylsilyl)-silylpotassium (obtained from tetrakis(trimethylsilyl)silane (30.0 g, 93.5 mmol) and KO^{t}Bu (11.0 g, 98.0 mmol)) in toluene (100 mL) dropwise. After it was stirred for 1 h, the reaction mixture was transferred to 0.5 M H_2SO_4/ice (300 mL) and extracted with diethyl ether (3 × 150 mL). The organic layers were dried over Na_2SO_4, and the solvent was removed. After recrystallization from diethyl ether colorless **7** (28.5 g, 97%) was obtained. Mp: 183−185 °C. ^1H NMR (δ in ppm): 0.53 (s, 12H, $SiMe_2$), 0.33 (s, 54H, $SiMe_3$). ^{13}C NMR (δ in ppm): 8.7 ($SiMe_2$), 3.1 ($SiMe_3$). ^{29}Si NMR (δ in ppm): 13.4 ($SiMe_2$), −10.5 ($SiMe_3$), −132.8 (Si_q).

1,3-Bis[potassiobis(trimethylsilyl)silyl]-1,1,3,3-tetramethyl-disiloxane (8). A solution of **7** (1 equiv) and KO^{t}Bu (2.05 equiv) in THF was stirred at 60 °C for 2 h. After complete conversion, THF was removed and replaced by toluene. ^1H NMR (δ in ppm): 0.69 (s, 12H, $SiMe_2$), 0.44 (s, 54H, $SiMe_3$). ^{13}C NMR (δ in ppm): 11.1 ($SiMe_2$), 7.2 ($SiMe_3$). ^{29}Si NMR (δ in ppm): 27.6 ($SiMe_2$), −7.0 ($SiMe_3$), −185.7 (SiK).

Synthesis of 9 by reaction of $[K(Me_3Si)_2Si]_2O$ (8) with $YbI_2{\cdot}(THF)_2$. To a suspension of $YbI_2{\cdot}(THF)_2$ (69 mg, 0.13 mmol) in toluene (2 mL) was added a solution of **8** (0.12 mmol) in toluene (2 mL) dropwise under strict exclusion of light. After 1 h the solvent volume was reduced, and the residue was treated with pentane (3 × 6 mL) and filtered over Celite. The solution volume was again reduced to 4 mL and stored at −37 °C for 24 h, after which yellow-orange crystalline **9** (87 mg, 86%) was obtained. Mp: 130−132 °C. ^1H NMR (δ in ppm): 3.68 (bs, 12H, THF), 1.32 (bs, 12H, THF), 0.67 (s, 12H, $SiMe_2$), 0.50 (s, 36H, $SiMe_3$). ^{13}C NMR (δ in ppm): 68.7 (THF), 25.2 (THF), 9.7 ($SiMe_2$), 6.4 ($SiMe_3$). ^{29}Si NMR (δ in ppm): 32.4 ($^2J_{Yb-Si}$ = 47 Hz, $SiMe_2$), −5.0 ($^2J_{Yb-Si}$ = 25 Hz, $SiMe_3$), −153.8 ($^1J_{Yb-Si}$ = 531 Hz, SiYb).

Synthesis of 10 by Reaction of $[K(Me_3Si)_2Si]_2O$ (8) with $SmI_2{\cdot}(THF)_2$. Compound **10** was obtained following the procedure for **9** (using **7** (100 mg, 0.16 mmol), KO^{t}Bu (37 mg, 0.33 mmol), and $SmI_2{\cdot}(THF)_2$ (92 mg, 0.17 mmol)) to yield **10** as dark green crystals (93 mg, 69%). Mp: 147−148 °C. ^1H NMR (δ in ppm): 3.65 (m, 12H, THF), 2.30 (m, 12H, THF), 0.23 (s, 36H, $SiMe_3$), −3.04 (s, 12H, $SiMe_2$). ^{13}C NMR (δ in ppm): 67.4 (THF), 28.4 ($SiMe_2$), 24.1 (THF), −16.1 ($SiMe_3$). ^{29}Si NMR (δ in ppm): 117.2 (SiSm), −118.1 ($SiMe_3$), n.d. ($SiMe_2$).

2,5-Dimethoxy-2,5-bis(trimethylsilyl)decamethylhexasilane (14). A solution of 2,2,5,5-tetrakis(trimethylsilyl)decamethylhexasilane (889 mg, 2.53 mmol) in CCl_4 (3 mL) and pentane (3 mL) was stirred for 48 h. After completion of conversion was checked by ^{29}Si NMR spectroscopy, triethylamine (1.0 mL) and DME (10 mL) were added followed by methanol (0.5 mL). After 15 min the solvent was removed and the residue was extracted with pentane (3 × 10 mL). After removal of the pentane, compound **14** was obtained as a colorless oil (843 mg, 84%). ^1H NMR (δ in ppm): 3.30 (s, 6H, OCH_3), 0.48 (s, 12H, $SiMe_2$), 0.29 (s, 36H, $SiMe_3$). ^{13}C NMR (δ in ppm): 55.8 (CH_3O), 1.2 ($SiMe_3$), −2.2 ($SiMe_2$). ^{29}Si NMR (δ in ppm): 9.8 (SiO), −15.1 ($SiMe_3$), −36.7 ($SiMe_2$).

2,5-Bis(methoxymethyl)-2,5-bis(trimethylsilyl)-decamethylhexasilane (16). To a solution of methoxymethyl chloride (67 mg, 0.83 mmol) in DME (2 mL) was added silanide **15** (obtained from 2,2,5,5-tetrakis(trimethylsilyl)decamethylhexasilane (250 mg, 0.41 mmol) and KO^{t}Bu (94 mg, 0.84 mmol)) dropwise, whereupon formation of a white precipitate occurred. After 15 min the solvent was removed and the residue was extracted with pentane (3 × 5 mL). After removal of pentane, compound **16** was obtained as a colorless oil (208 mg, 92%). ^1H NMR (δ in ppm): 3.47 (s, 4H, $SiCH_2$), 3.15 (s, 6H, OCH_3), 0.48 (s, 12H, $SiMe_2$), 0.31 (s, 36H, $SiMe_3$). ^{13}C NMR (δ in ppm): 63.0 (CH_3OCH_2), 1.8 ($SiMe_3$), −1.2 ($SiMe_2$). ^{29}Si NMR (δ in ppm): −12.2 ($SiMe_3$), −34.8 ($SiMe_2$), −77.5 ($SiCH_2OCH_3$).

DOI: 10.1021/acs.inorgchem.7b00420
Inorg. Chem. 2017, 56, 5328−5341

1-Methoxy-3,3-bis(trimethylsilyl)heptamethyltetrasilane (17). To a solution of $(Me_3Si)_3Si\text{-}Me_2Si\text{-}SiMe_2Cl$ (300 mg, 0.75 mmol) and NEt_3 (1 mL) in DME (4 mL) was added methanol (1 mL) dropwise. After 2 h the solvent was removed and the residue extracted with pentane (3 × 5 mL). The solvent was removed, and the colorless semisolid **17** (296 mg, 99%) was obtained. ^{1}H NMR (δ in ppm): 3.22 (s, 3H, OCH_3), 0.33 (s, 6H, $SiMe_2$), 0.31 (s, 27H, $SiMe_3$), 0.24 (s, 6H, $OSiMe_2$). ^{13}C NMR (δ in ppm): 50.0 (CH_3O), 3.2 ($SiMe_3$), −0.5 ($OSiMe_2$), −1.2 ($SiMe_2$). ^{29}Si NMR (δ in ppm): 17.7 (Me_2SiO), −9.6 ($SiMe_3$), −42.2 ($SiMe_2$), −133.0 (Si_q).

Bis[2-methoxy-1,1,2,2-tetrakis(trimethylsilyl)disilanyl]-ytterbium−THF (19). The same procedure as for **3** was used, employing $YbI_2\cdot(THF)_2$ (97 mg, 0.17 mmol), **18** (100 mg, 0.36 mmol), and KO^{t}Bu (40 mg, 0.36 mmol) in toluene. After recrystallization from pentane at −37 °C yellow crystalline **19** (71 mg, 79%) was obtained. Mp: 177−181 °C. ^{1}H NMR (δ in ppm, C_6D_6): 3.74 (bs, 4H, THF), 3.47 (s, 6H, OMe), 1.41 (bs, 4H, THF), 0.51 (s, 36H, $YbSiSiMe_3$), 0.39 (s, 36H, $OSiSiMe_3$). ^{13}C NMR (δ in ppm, C_6D_6): 69.0 (THF), 56.7 (OMe), 25.2 (THF), 7.2 ($YbSiSiMe_3$), 2.2 ($OSiSiMe_3$). ^{29}Si NMR (δ in ppm, C_6D_6): 34.1 (MeOSi), −6.7 ($YbSiSiMe_3$), −16.1 ($OSiSiMe_3$), −134.7 (SiYb).

Synthesis of $MeN(CH_2CH_2O)_2SiMeCl$ (20). $MeN(CH_2CH_2OSiMe_3)_2$ (1.16 g, 4.32 mmol) and $MeSiCl_3$ (679 mg, 4.54 mmol) were dissolved in toluene (6 mL) and heated to reflux for 20 h. Colorless crystalline **20** (563 mg, 69%) was obtained by decantation. Mp: 128−131 °C. ^{1}H NMR (δ in ppm, $CDCl_3$): 3.89 (m, 4H, OCH_2), 2.86 (quintet, J_{H-H} = 6.1 Hz, 2H, NCH_2), 2.66 (quintet, J_{H-H} = 6.1 Hz, 2H, NCH_2), 2.46 (s, 3H, NCH_3), 0.55 (s, 3H, $SiCH_3$). ^{13}C NMR (δ in ppm, $CDCl_3$): 59.7 (OCH_2), 54.6 (NCH_2), 43.6 (MeN), 3.9 (MeSi). ^{29}Si NMR (δ in ppm, $CDCl_3$): −56.3. Anal. Calcd for $C_6H_{14}ClNO_2Si$ [195.72]: C, 36.82; H, 7.21; N, 7.16. Found: C, 37.16; H, 7.12; N, 7.25.

1,1-Methylaminobis(ethyloxy)-2,2-bis(trimethylsilyl)-tetramethyltrisilane (21). To a solution of **20** (315 mg, 1.605 mmol) in toluene (1 mL) was added tris(trimethylsilyl)silylpotassium (obtained from tetrakis(trimethylsilyl)silane (500 mg, 1.558 mmol) and KO^{t}Bu (180 mg, 1.605 mmol) in DME; after complete conversion, DME was removed and replaced by toluene) in toluene (5 mL). After it was stirred for 5 h, the solution mixture was filtered, the precipitate washed with pentane, and the solvent from the combined organic layers removed. After recrystallization from pentane at −57 °C colorless crystalline **21** (373 mg, 61%) was obtained. Mp: 45−50 °C. ^{1}H NMR (δ in ppm, $CDCl_3$): 3.71 (m, 4H, OCH_2), 2.56 (t, J_{H-H} = 4.5 Hz, 4H, NCH_2), 2.41 (s, 3H, CH_3N), 0.31 (s, 3H, $SiCH_3$), 0.19 (s, 27H, $(CH_3)_3Si$). ^{13}C NMR (δ in ppm, $CDCl_3$): 62.3 (OCH_2), 58.3 (NCH_2), 44.3 (MeN), 3.7 (MeSi), 2.4 [$(Me_3Si)_3$-Si]. ^{29}Si NMR (δ in ppm, $CDCl_3$): 3.5 (SiO_2), −10.1 (Me_3Si), −134.8 [$(Me_3Si)_3Si$]. Anal. Calcd for $C_{15}H_{41}NO_2Si_5$ [407.92]: C, 44.17; H, 10.13; N, 3.43. Found: C, 44.24; H, 9.63; N, 3.41.

Silocane−Yb Complex 22. The same procedure was used as for the preparation of **3** with $YbI_2\cdot(THF)_2$ (56 mg, 0.10 mmol), **21** (80 mg, 0.20 mmol), and KO^{t}Bu (23 mg, 0.21 mmol) (silanide **21a**: ^{29}Si NMR (δ in ppm, D_2O capillary) 35.9 ($MeSiO_2$), −5.4 ($SiMe_3$), −210.2 (SiYb)). The formation of the silanide was carried out in DME, which after complete conversion was replaced by toluene. After recrystallization from pentane at −37 °C yellow crystalline **22** (36 mg, 43%) was obtained. Mp: 143−144 °C dec. ^{1}H NMR (δ in ppm, C_6D_6): 3.70 (m, 4H, OCH_2), 2.12 (s, 3H, NCH_3), 1.79 (bs, 4H, NCH_2), 0.54 (s, 21H, $SiMe_2$ and $SiMe_3$). ^{13}C NMR (δ in ppm, C_6D_6): 80.4 (OCH_2), 60.9 (bs, NCH_2), 47.9 (NCH_3), 6.3 ($SiMe_3$), 4.0 (SiMe). ^{29}Si NMR (δ in ppm, C_6D_6): 38.8 ($MeSiO_2$), −5.0 ($SiMe_3$), −182.0 (SiYb).

Silocane−Eu Complex 23. The same procedure as for **3** was used with $EuI_2\cdot(THF)_2$ (169 mg, 0.31 mmol), **21** (228 mg, 0.56 mmol), and KO^{t}Bu (66 mg, 0.58 mmol). The reaction to the anion was done in DME, which was after complete conversion replaced by toluene. After recrystallization with pentane at −37 °C green crystalline **23** (48 mg, 21%) was obtained. Mp: 185−190 °C. NMR: not detectable. Anal. Calcd for $C_{24}H_{64}EuN_2O_4Si_8$ [821.43]: C, 35.09; H, 7.85; N, 3.41. Found: C, 34.92; H, 7.81; N, 3.43.

■ ASSOCIATED CONTENT

Supporting Information

The Supporting Information is available free of charge on the ACS Publications website at DOI: 10.1021/acs.inorgchem.7b00420.

^{1}H, ^{13}C{^{1}H}, ^{29}Si{^{1}H} INEPT, and various 2-D NMR spectra of compounds **2**, **3**, **7**−**10**, **14**, **16**, **19**, **21a**, and **22**, ORTEP and packing plots of **3**, **7**, **10**, **20**, **22**, and **23**, energy level plots of **23** and Cartesian coordinates of **2**, **4**, and **23** (PDF)

Crystallographic data for **2**−**4**, **8**, **9**, **10**, **19**, **20**, **22**, and **23** (CIF)

Cartesian coordinates of **2**, **4**, and **23** (XYZ)

■ AUTHOR INFORMATION

Corresponding Authors

*E-mail for H.K.: heinz.krenn@uni-graz.at.
*E-mail for C.M.: christoph.marschner@tugraz.at.
*E-mail for T.S.: szilvasi@wisc.edu.
*E-mail for J.B.: baumgartner@tugraz.at.

ORCID

Christoph Marschner: 0000-0001-8586-2889
Judith Baumgartner: 0000-0002-9938-1813

Funding

Support for this study was provided by the Austrian *Fonds zur Förderung der wissenschaftlichen Forschung* (FWF) via the projects P-25124 (J.B.) and P-26417 (C.M.).

Notes

The authors declare no competing financial interest.

■ ACKNOWLEDGMENTS

The authors gratefully acknowledge Dr. Ulrich Flörke (University of Paderborn) for discussion and advice concerning the crystallographic analysis of compound **6**.

■ REFERENCES

(1) Evans, W. J. The Importance of Questioning Scientific Assumptions: Some Lessons from f Element Chemistry. *Inorg. Chem.* **2007**, *46*, 3435−3449.

(2) Evans, W. J. The expansion of divalent organolanthanide reduction chemistry via new molecular divalent complexes and sterically induced reduction reactivity of trivalent complexes. *J. Organomet. Chem.* **2002**, *647*, 2−11.

(3) MacDonald, M. R.; Bates, J. E.; Ziller, J. W.; Furche, F.; Evans, W. J. Completing the Series of + 2 Ions for the Lanthanide Elements: Synthesis of Molecular Complexes of Pr^{2+}, Gd^{2+}, Tb^{2+}, and Lu^{2+}. *J. Am. Chem. Soc.* **2013**, *135*, 9857−9868.

(4) Fieser, M. E.; MacDonald, M. R.; Krull, B. T.; Bates, J. E.; Ziller, J. W.; Furche, F.; Evans, W. J. Structural, Spectroscopic, and Theoretical Comparison of Traditional vs Recently Discovered Ln^{2+} Ions in the $[K(2.2.2\text{-cryptand})][(C_5H_4SiMe_3)_3Ln]$ Complexes: The Variable Nature of Dy^{2+} and Nd^{2+}. *J. Am. Chem. Soc.* **2015**, *137*, 369−382.

(5) Evans, W. J. Tutorial on the Role of Cyclopentadienyl Ligands in the Discovery of Molecular Complexes of the Rare-Earth and Actinide Metals in New Oxidation States. *Organometallics* **2016**, *35*, 3088−3100.

(6) Zitz, R.; Hlina, J.; Gatterer, K.; Marschner, C.; Szilvási, T.; Baumgartner, J. Neutral "Cp-Free" Silyl-Lanthanide(II) Complexes: Synthesis, Structure, and Bonding Analysis. *Inorg. Chem.* **2015**, *54*, 7065−7072.

(7) Fischer, R.; Frank, D.; Gaderbauer, W.; Kayser, C.; Mechtler, C.; Baumgartner, J.; Marschner, C. α,ω-Oligosilyl Dianions and Their

DOI: 10.1021/acs.inorgchem.7b00420
Inorg. Chem. 2017, 56, 5328−5341

Application in the Synthesis of Homo- and Heterocyclosilanes. *Organometallics* **2003**, *22*, 3723−3731.
(8) Kayser, C.; Kickelbick, G.; Marschner, C. Simple Synthesis of Oligosilyl-α,ω-dipotassium Compounds. *Angew. Chem., Int. Ed.* **2002**, *41*, 989−992.
(9) Kayser, C.; Fischer, R.; Baumgartner, J.; Marschner, C. Tailor-made Oligosilyl Potassium Compounds. *Organometallics* **2002**, *21*, 1023−1030.
(10) Frank, D.; Baumgartner, J.; Marschner, C. First successful reaction of a silyl anion with hafnium tetrachloride. *Chem. Commun.* **2002**, 1190−1191.
(11) Likhar, P. R.; Zirngast, M.; Baumgartner, J.; Marschner, C. Preparation and structural characterisation of methoxybis-(trimethylsilyl)silyl potassium and its condensation product. *Chem. Commun.* **2004**, 1764−1765.
(12) Tamao, K.; Kawachi, A. The Chemistry of Silylenoids: Preparation and Reactivity of (Alkoxysilyl)lithium Compounds. *Angew. Chem., Int. Ed. Engl.* **1995**, *34*, 818−820.
(13) Fischer, R.; Konopa, T.; Baumgartner, J.; Marschner, C. Small Cyclosilanes: Syntheses and Reactions toward Mono- and Dianions. *Organometallics* **2004**, *23*, 1899−1907.
(14) Gaderbauer, W.; Zirngast, M.; Baumgartner, J.; Marschner, C.; Tilley, T. D. Synthesis of Polysilanylmagnesium Compounds. *Organometallics* **2006**, *25*, 2599−2606.
(15) Gaderbauer, W.; Balatoni, I.; Wagner, H.; Baumgartner, J.; Marschner, C. Synthesis and structural diversity of oligosilanylzinc compounds. *Dalton Trans.* **2010**, *39*, 1598−1603.
(16) Corradi, M. M.; Frankland, A. D.; Hitchcock, P. B.; Lappert, M. F.; Lawless, G. A. Synthesis, structure and reactivity of $[Yb(\eta\text{-}C_5Me_5)\{Si(SiMe_3)_3\}(thf)_2]$. *Chem. Commun.* **1996**, 2323−2324.
(17) Niemeyer, M. Reactions of Hypersilyl Potassium with Rare-Earth Metal Bis(Trimethylsilylamides): Addition versus Peripheral Deprotonation. *Inorg. Chem.* **2006**, *45*, 9085−9095.
(18) Thalangamaarachchige, V. D.; Unruh, D. K.; Cordes, D. B.; Krempner, C. Synthesis, Structure, and Reactivity of Zwitterionic Divalent Rare-Earth Metal Silanides. *Inorg. Chem.* **2015**, *54*, 4189−4191.
(19) Marschner, C. Preparation and Reactions of Polysilanyl Anions and Dianions. *Organometallics* **2006**, *25*, 2110−2125.
(20) Spek, A. L. *PLATON* SQUEEZE: a tool for the calculation of the disordered solvent contribution to the calculated structure factors. *Acta Crystallogr., Sect. C: Struct. Chem.* **2015**, *71*, 9−18.
(21) Massarweh, G.; Fischer, R. D. Umlagerung von Tetrahydrofuran im Lanthanoid-Organyl: Die Kristall- und Molekülstrukturen von Bis(cyclopentadienyl)ytterbium(III) (μ-n-buten-2-olat) und Bis-(methylclopentadienyl)ytterbium(III) (μ-η^2:η^1-tetrahydrofuran-2-olat). *J. Organomet. Chem.* **1993**, *444*, 67−74.
(22) Evans, W. J.; Perotti, J. M.; Ziller, J. W.; Moser, D. F.; West, R. Evaluation of a Silylene Divalent Lanthanide Interaction in the Metallocene Complex $(C_5Me_5)_2Sm[SiN^tBuCHCHN^tBu]$. *Organometallics* **2003**, *22*, 1160−1163.
(23) Radu, N. S.; Hollander, F. J.; Tilley, T. D.; Rheingold, A. L. Samarium-mediated redistribution of silanes and formation of trinuclear samarium-silicon clusters. *Chem. Commun.* **1996**, 2459−2460.
(24) Cordero, B.; Gómez, V.; Platero-Prats, A. E.; Revés, M.; Echeverría, J.; Cremades, E.; Barragán, F.; Alvarez, S. Covalent radii revisited. *Dalton Trans.* **2008**, 2832−2838.
(25) Song, J.-I.; Gambarotta, S. The First Dinuclear Low-Valent Samarium Complex with a Short Sm−Sm Contact. *Angew. Chem., Int. Ed. Engl.* **1995**, *34*, 2141−2143.
(26) Wang, K. G.; Stevens, E. D.; Nolan, S. P. Synthesis and structural characterization of a tetranuclear organolanthanide hydrazido complex. *Organometallics* **1992**, *11*, 1011−1013.
(27) Dubé, T.; Conoci, S.; Gambarotta, S.; Yap, G. P. A. Divalent and Mixed-Valence Samarium Clusters Supported by Dipyrrolide Ligand. *Organometallics* **2000**, *19*, 1182−1185.
(28) Steudel, A.; Siebel, E.; Fischer, R. D.; Paolucci, G.; Lucchini, V. Bis(cyclopentadienyl)lanthanoid(III) alkoxides derived from chiral alcohols with a nitrogen donor functionality: Solution NMR studies of paramagnetic complexes. *J. Organomet. Chem.* **1998**, *556*, 229−238.
(29) Satoh, Y.; Ikitake, N.; Nakayama, Y.; Okuno, S.; Yasuda, H. Syntheses of bis- and tetra(trimethylsilyl) substituted lanthanocene methyl complexes and their catalyses for polymerizations of methyl methacrylate, ϵ-caprolactone and l-lactide. *J. Organomet. Chem.* **2003**, *667*, 42−52.
(30) Wang, Q.; Xiang, L.; Song, H.; Zi, G. Synthesis of Amidolanthanides with New Chiral Biaryl-Based NNO Ligands and Their Use as Catalysts for Enantioselective Hydroamination/Cyclization. *Inorg. Chem.* **2008**, *47*, 4319−4328.
(31) *International Tables for Cystallography*; Hahn, T., Shmueli, U., Wilson, A. J. C., International Union of Crystallography, Eds.; D. Reidel: Dordrecht, Holland, 1984.
(32) Pestunovich, V.; Kirpichenko, S.; Voronkov, M. Silatranes and Their Tricyclic Analogs. In *The Chemistry of Organic Silicon Compounds*; Rappoport, Z., Apeloig, Y., Eds.; Wiley: Chichester, U.K., 2003; pp 1447−1537.
(33) Voronkov, M. G.; Brodskaya, E. I.; Belyaeva, V. V.; Chuvashev, D. D.; Toryashinova, D. D.; Ermikov, A. F.; Baryshok, V. P. Through-bond interaction in compounds containing an Si-O-C-C-N group. *J. Organomet. Chem.* **1986**, *311*, 9−16.
(34) Yan, K.; Upton, B. M.; Ellern, A.; Sadow, A. D. Lewis Acid-Mediated β-Hydride Abstraction Reactions of Divalent $M(C(SiHMe_2)_3)_2THF_2$ (M = Ca, Yb). *J. Am. Chem. Soc.* **2009**, *131*, 15110−15111.
(35) Yan, K.; Schoendorff, G.; Upton, B. M.; Ellern, A.; Windus, T. L.; Sadow, A. D. Intermolecular β-Hydrogen Abstraction in Ytterbium, Calcium, and Potassium Tris(dimethylsilyl)methyl Compounds. *Organometallics* **2013**, *32*, 1300−1316.
(36) Chen, Y.; Song, H.; Cui, C. Dehydrosilylation of $ArNHSiH_3$ with Ytterbium(II) Amide: Formation of a Dimeric Ytterbium(II) Silanimine Complex. *Angew. Chem., Int. Ed.* **2010**, *49*, 8958−8961.
(37) Hou, Z.; Zhang, Y.; Nishiura, M.; Wakatsuki, Y. (Pentamethylcyclopentadienyl)lanthanide(II) Alkyl and Silyl Complexes: Synthesis, Structures, and Catalysis in Polymerization of Ethylene and Styrene. *Organometallics* **2003**, *22*, 129−135.
(38) Zitz, R.; Arp, H.; Hlina, J.; Walewska, M.; Marschner, C.; Szilvási, T.; Blom, B.; Baumgartner, J. Open-Shell Lanthanide(II+) or -(III+) Complexes Bearing σ-Silyl and Silylene Ligands: Synthesis, Structure, and Bonding Analysis. *Inorg. Chem.* **2015**, *54*, 3306−3315.
(39) Kahn, O. In *Molecular magnetism*; Wiley-VCH: New York, 1993; pp 47−52.
(40) Pangborn, A. B.; Giardello, M. A.; Grubbs, R. H.; Rosen, R. K.; Timmers, F. J. Safe and Convenient Procedure for Solvent Purification. *Organometallics* **1996**, *15*, 1518−1520.
(41) Lukens, W. W.; Matsunaga, P. T.; Andersen, R. A. Synthesis and Structure of Cp^*_2TiH, $Cp^*_2TiH_2Li(tmed)$, and $[Cp^*_2TiOLi(THF)]_2$. *Organometallics* **1998**, *17*, 5240−5247.
(42) Wallner, A.; Wagner, H.; Baumgartner, J.; Marschner, C.; Rohm, H. W.; Kockerling, M.; Krempner, C. Structure, Conformation, and UV Absorption Behavior of Partially Trimethylsilylated Oligosilane Chains. *Organometallics* **2008**, *27*, 5221−5229.
(43) Girard, P.; Namy, J. L.; Kagan, H. B. Divalent lanthanide derivatives in organic synthesis. 1. Mild preparation of samarium iodide and ytterbium iodide and their use as reducing or coupling agents. *J. Am. Chem. Soc.* **1980**, *102*, 2693−2698.
(44) *Synthetic Methods of Organometallic and Inorganic Chemistry*; Herrmann, W. A., Brauer, G., Eds.; Georg Thieme Verlag and Thieme Medical Publishers: Stuttgart, New York, 1996.
(45) Evans, W. J.; Grate, J. W.; Choi, H. W.; Bloom, I.; Hunter, W. E.; Atwood, J. L. Solution synthesis and crystallographic characterization of the divalent organosamarium complexes $(C_5Me_5)_2Sm(THF)_2$ and $[(C_5Me_5)Sm(\mu\text{-}I)(THF)_2]_2$. *J. Am. Chem. Soc.* **1985**, *107*, 941−946.
(46) Morris, G. A.; Freeman, R. Enhancement of nuclear magnetic resonance signals by polarization transfer. *J. Am. Chem. Soc.* **1979**, *101*, 760−762.

DOI: 10.1021/acs.inorgchem.7b00420
Inorg. Chem. 2017, 56, 5328−5341

(47) Helmer, B. J.; West, R. Enhancement of ^{29}Si NMR Signals by Proton Polarization Transfer. *Organometallics* **1982**, *1*, 877−879.
(48) *SAINTPLUS: Software Reference Manual, Version 6.45*, Bruker-AXS: Madison, WI, 1997−2003.
(49) Blessing, R. H. An empirical correction for absorption anisotropy. *Acta Crystallogr., Sect. A: Found. Crystallogr.* **1995**, *51*, 33−38.
(50) Sheldrick, G. M. *SADABS, Version 2.10*; Bruker AXS Inc., Madison, WI, 2003.
(51) Sheldrick, G. M. A short history of SHELX. *Acta Crystallogr., Sect. A: Found. Crystallogr.* **2008**, *64*, 112−122.
(52) Farrugia, L. J. *WinGX* and *ORTEP* for *Windows*: an update. *J. Appl. Crystallogr.* **2012**, *45*, 849−854.
(53) *POVRAY 3.6*; Persistence of Vision Pty. Ltd., Williamstown, Victoria, Australia, 2004; available online at http://www.povray.org/download/ (accessed on 09.07.2008).

DOI: 10.1021/acs.inorgchem.7b00420
Inorg. Chem. 2017, 56, 5328−5341